Nanoscale Res Lett (2010) 5:489–493
DOI 10.1007/s11671-010-9549-6

SPECIAL ISSUE ARTICLE

Study on Composition Distribution and Ferromagnetism of Monodisperse FePt Nanoparticles

H. B. Wang · H. Wang · J. Zhang · F. J. Yang · Y. M. Xu · Q. Li

Received: 11 August 2009 / Accepted: 18 January 2010 / Published online: 4 February 2010

Abstract Monodisperse FePt nanoparticles with size of 4.5 and 6.0 nm were prepared by simultaneous reduction of platinum acetylacetonate and thermal decomposition of iron pentacarbonyl in benzylether. The crystallography structure, size, and composition of the FePt nanoparticles were examined by X-ray diffraction and transmission electron microscopy. Energy dispersive X-ray spectrometry measurements of individual particles indicate a broad compositional distribution in both the 4.5 and 6 nm FePt nanoparticles. The effects of compositional distribution on the phase-transition and magnetic properties of the FePt nanoparticles were investigated.

Keywords FePt · Nanoparticles · Compositional distribution · Magnetic properties

Introduction

Chemical synthesized FePt nanoparticles (NPs) have attracted much research interest because of their potential application in ultrahigh density magnetic recording media, bio-medical application and catalyst [1–3]. FePt has two phases, one is fcc and the other is fct. Fcc is the commonly obtained format, soft magnet and can transform to hard-magnetic fct phase at high temperatures. Since IBM group demonstrated a hot organometallic synthesis for the monodisperse fcc FePt NPs in 2000, the method was subsequently developed by many groups aiming at achieving FePt nanoparticles with controlled size, shape, self-assemblies as well as functional composite structures [4–10]. Although many progresses were made in this area, there have been relatively limited investigations on the formation mechanism of the FePt NPs. For instance, a wide atomic composition distribution was reported in the 3.1 nm FePt NPs by Yu et al. [11]. Such a broad compositional distribution was recently observed in the 2.9 nm FePt NPs by Thompson et al. [12] and 4.6 nm FePt NPs by Bagaria et al. [13]. However, the composition distribution of bigger (larger than 5 nm) FePt NPs is not clear yet. It's well known that the particle-to-particle compositional variation would significantly affect the phase transition as well as magnetic performance of the FePt system. To understand the mechanism of the formation of FePt NPs and their magnetic properties, an insight into the atomic composition of the FePt NPs is of significance.

In this study, we focus on the atomic composition and magnetic properties of FePt nanoparticles prepared by organic solution method. Monodisperse FePt NPs were synthesized via simultaneous reduction of platinum acetylacetonate and thermo-decomposition of iron pentacarbonyl in benzylether using oleyl amine and oleic acid as surfactants. The size and composition of the nanoparticles were tuned by changing the dose of $Fe(CO)_5$ and surfactants (oleyl amine and oleic acid) in the reactions. After systematically examined the isolated FePt nanoparticles using TEM-EDX, we observed an inhomogeneous compositional distribution in both the 4.5 and 6.0 nm equiatomic FePt NPs. It was also found that the 6 nm $Fe_{50}Pt_{50}$ nanoparticles have wider composition distribution than that of the 4.5 nm $Fe_{48}Pt_{52}$ NPs. This is attributed to the wider size distribution of Pt nuclei in the formation of bigger FePt

H. B. Wang · H. Wang (✉) · J. Zhang · F. J. Yang
Faculty of Physics and Electronic Technology, Hubei University, 430062 Wuhan, People's Republic of China
e-mail: nanoguy@126.com

Y. M. Xu · Q. Li
Department of Physics, The Chinese University of Hong Kong, Hong Kong, People's Republic of China

nanoparticles. The effects of composition variation on the magnetic properties of the FePt nanoparticles are discussed.

Experimental

The FePt nanoparticles were prepared by slightly modify the synthesis procedure reported by Chen [14]. In the synthesis of 4.5 nm FePt NPs, 0.5 mmol platinum acetylacetonate ($Pt(acac)_2$) was added to a flask and mixed with 20 ml benzyl ether under a nitrogen atmosphere. After the solution was stirred for 15 min at room temperature, the flask was heated up to 100°C and then 1 mmol oleic acid, 1 mmol oleylamine and 2 mmol $Fe(CO)_5$ were added. The heat rate was keeping at 5°C/min during the synthesis. The solution was then directly heated to reflux temperature for 30 min before cooling to room temperature. Similar procedure was employed for the synthesis of 6 nm FePt NPs. In the reaction, the dose of $Fe(CO)_5$ was 2.5 and 2 mmol olcic acid, 2 mmol oleylamine were used while the other conditions were kept unchanged.

After the prepared black solution was cooled to the room temperature, 20 ml ethanol was added into the solution, the black products were then precipitated by mild centrifugation (5,000 rpm). The yellow–brown supernatant was discarded. The precipitate were redispersed in 10 ml hexane and precipitated again with 20 ml ethanol by centrifugation. Further purification of the product was performed by dispersing the product into hexane, precipitating it out with ethanol, and centrifuging. Finally, the purified nanoparticles were dispersed in mixture of 10 ml hexane.

The size and morphology of the nanoparticles are characterized using transmission electron microscopy (TEM, Tecnai 20 ST, FEG). The individual particle composition measurements by energy dispersive X-ray spectrometry (EDS) were performed on the FEI Tecnai STEM with a spot size of $\sim$2 nm. The crystallography structure of the FePt nanoparticle powder was characterized by X-ray diffraction (XRD, Bruker D5) with CuK_α radiation. The magnetic properties of the FePt nanoparticles were measured by a vibrating sample magnetometer (VSM) at 300 K.

Results and Discussion

Figure 1 shows the TEM images of the as-synthesized FePt nanoparticles. As can be seen from the figure, the nanoparticles are uniform and could display local ordered assembly on the carbon coated copper grid. The size of these particles in Fig. 1a and b is found to be 4.5 ± 0.27

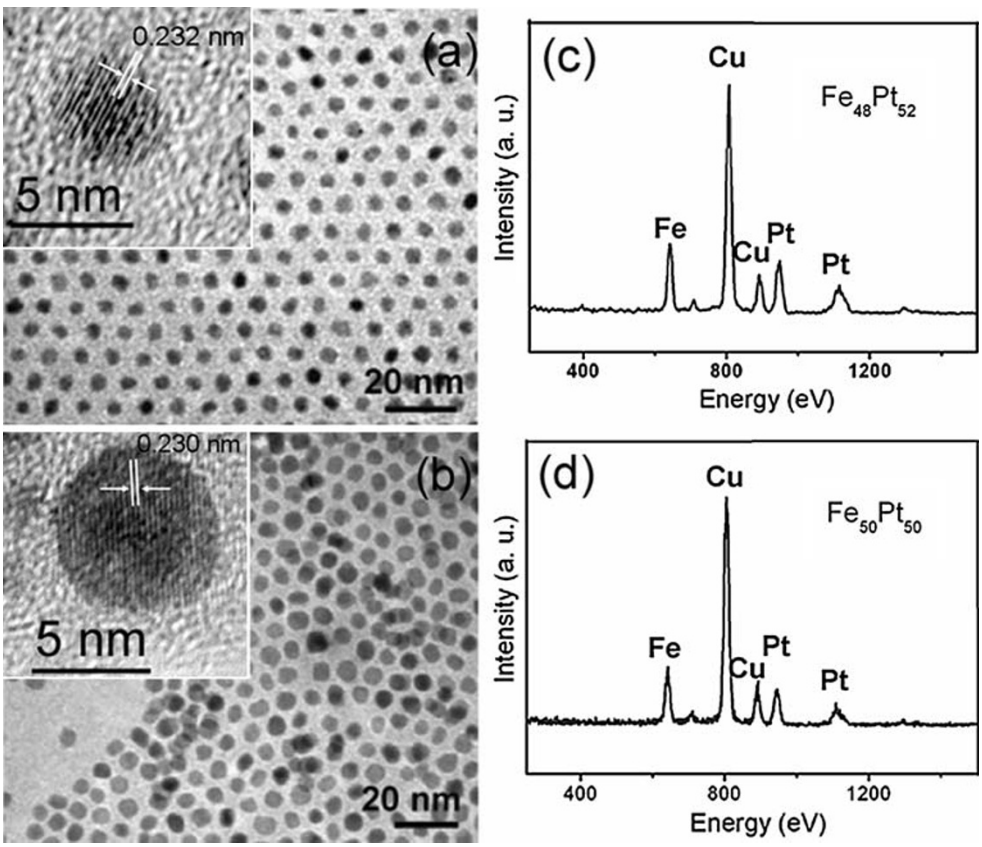

Fig. 1 TEM images of the **a** 4.5 nm and (b) 6.0 nm FePt nanoparticles, *insets* are the corresponding high resolution TEM images of the particles. **c**, **d** are EDX spectra of the FePt nanoparticles in **a** and **b**, respectively

and 6.0 ± 0.45 nm, respectively. The typical HRTEM images of both the 4.5 and 6.0 nm FePt nanoparticles are given as the inset of Fig. 1a and b. The measured inter-fringe distance is 0.232 and 0.230 nm, respectively, being close to the {111} lattice spacing of fcc FePt ($\sim$0.235 nm). The average composition of these NPs is obtained by the EDX with electron probe covering hundreds of such particles. Shown in Fig. 1c and d are the EDX spectra of the particles. The average composition of the nanoparticles is estimated to be $Fe_{48}Pt_{52}$ for the 4.5 nm NPs and $Fe_{50}Pt_{50}$ for the 6.0 nm NPs.

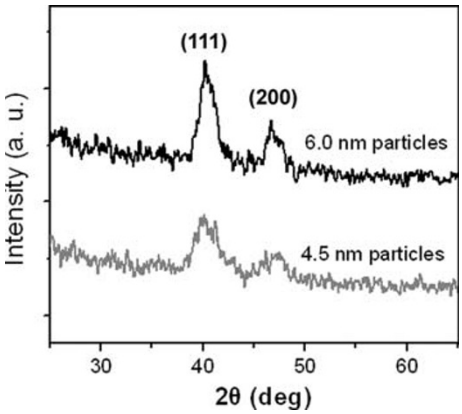

Fig. 2 XRD spectra of the as-synthesized 4.5 and 6.0 nm FePt nanoparticles

XRD spectra of the as-synthesized FePt nanoparticles are given in Fig. 2. The broad diffraction peaks centered at $\sim$40° and $\sim$46° are observed, which can be indexed to (111) and (002) planes of fcc structured FePt. The crystal size determined by the Debye–Scherre equation with XRD data is 6.1 and 4.3 nm for the two samples, agreeing with the particle sizes observed from TEM images.

We carried out atomic compositional analysis of the nanoparticles by examining the composition of individual particles. It's known that in the high-angle annular dark field (HAADF) image, the elements with higher atomic number will have brighter contrast compared to the light elements with lower atomic number [15]. Therefore, it's reasonable to assume that for the isolated FePt NPs, the brighter spots are corresponding to the Pt-rich particles while the darker spots are the Fe-rich ones, since Fe has a significantly lower atomic number than Pt. Figure 3a shows the HADDF image of the 4.5 nm NPs, the FePt NPs manifest different contrast in the figure. EDX spectra were

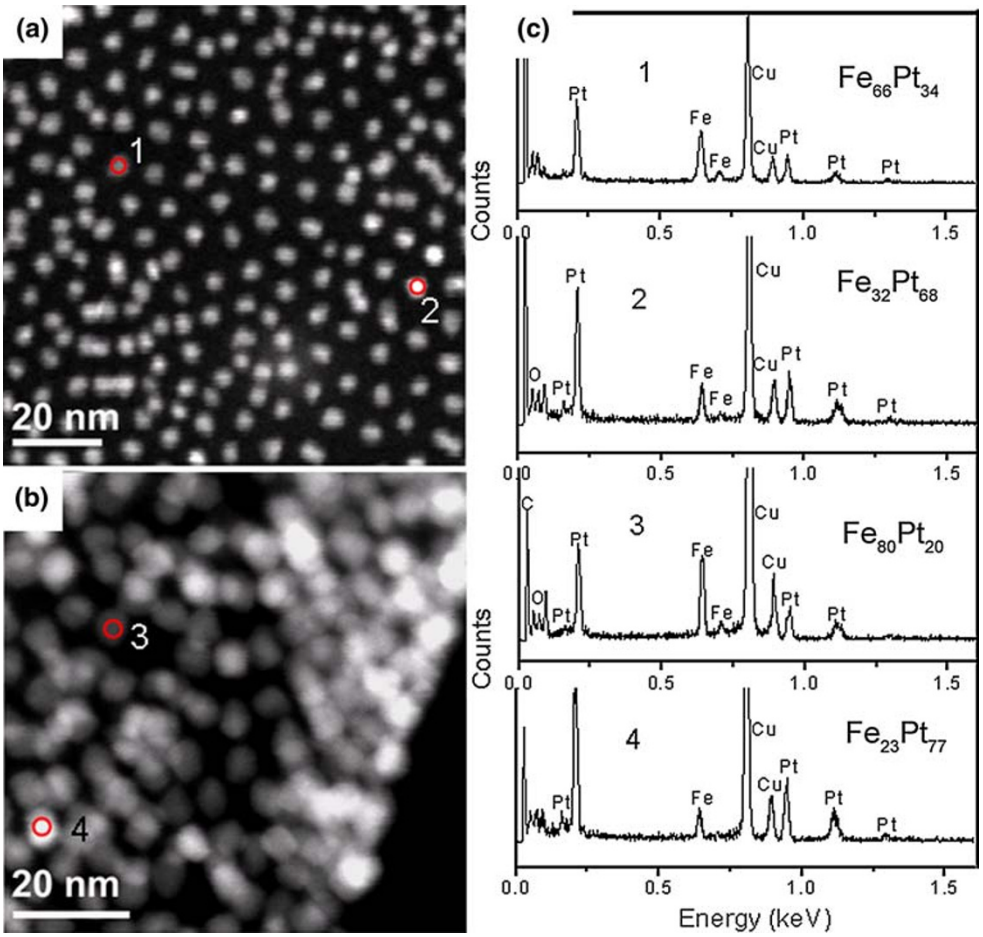

Fig. 3 STEM-high angle annular dark field (HAADF) images of **a** 4.5 nm FePt nanoparticles and **b** 6.0 nm FePt nanoparticles for TEM-EDS measurements. **c** EDX spectra of individual FePt nanoparticles with the electron probe circled in **a** and **b**

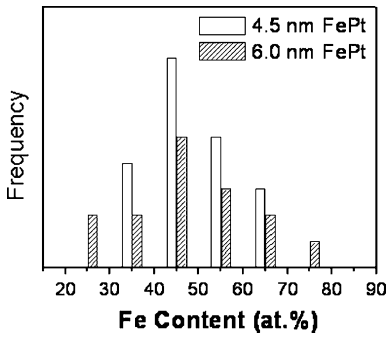

Fig. 4 Atomic composition distribution of 4.5 and 6.0 nm FePt nanoparticles by STEM-EDX measurements

obtained on both the brightest and darkest spots with electron beam (spot size is 2 nm) cover the corresponding isolated particles. Systematic measurements confirm that the brighter particles in the HADDF image are Pt rich while the darker particles are Fe-rich particles. In the measurements, the composition of the brightest nanoparticle is $Fe_{32}Pt_{68}$ and the darkest nanoparticle is $Fe_{66}Pt_{34}$ in the 4.5 nm FePt particles. The measured composition of other individual particles does not exceed this range. A rough statistics obtained based on twenty randomly selected NPs is given as a histogram in Fig. 4. From the histogram, there is about 65% of FePt NPs in the composition range of 40–60 atm% Fe. This value is higher than the value reported by Yu et al. [11] but lower than that reported by Saita et al. [16] by using iron ethoxide as the precursors.

The HADDF image of the 6.0 nm NPs is also presented in Fig. 3. Atomic composition between $Fe_{20}Pt_{80}$ and $Fe_{77}Pt_{23}$ were obtained by measuring fifteen isolated FePt NPs in this system. Though the analysis is not enough to give a histogram of the compositional distribution, an even wider composition variation is observed for the 6 nm FePt NPs. These results may be understood by the reaction mechanism of the FePt NPs. It has been demonstrated that the organometallic reaction involves the formation of a Pt (or Pt rich) seed cluster followed by further growth of Fe atoms onto the seed [7, 12, 17]. The composition variation of the FePt NPs can be caused by different size of Pt nuclei and un-homogenous supply of Fe source onto the Pt nuclei [16]. Specially, in the formation of bigger FePt NPs, more surfactants were used to lower nucleation rates of the Pt precursor and this may give rise to larger difference in the size of the Pt nuclei. Smaller Pt seeds have great surface specific area and allow more Fe atoms grow on them. Likewise, less Fe atoms would grow onto the bigger Pt seeds to form a Pt rich FePt nanoparticle. Consequently, a wide composition distribution is formed due to the separation of nucleation and growth of FePt NPs in reaction.

It's known that for each fcc-structured FePt NP, the atomic composition should be within 40–60% Fe to allow

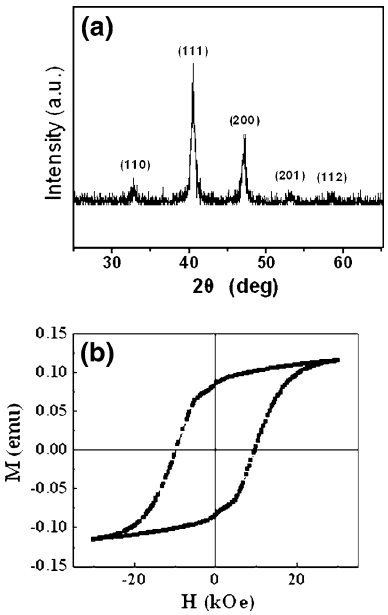

Fig. 5 **a** XRD pattern and **b** room-temperature hysteresis loop of the 6 nm $Fe_{50}Pt_{50}$ nanoparticles after annealing at 600°C for 1 h

its transformation into the fct phase [18]. Therefore, the atomic composition distribution has an impact on the whole magnetic properties of the FePt NPs since a portion of Fe_xPt_{100-x} NPs fall beyond the composition range of $40 < x < 60$. The effects of composition distribution on the phase transition as well as ferromagnetism of FePt NPs (3.1 nm) were studied by Yu et al. [11]. They found that the sintered FePt NPs due to thermal annealing exhibited high coercivity while the separated ones showed very low coercivity. Such difference is attributed to the large composition distribution and size effect of the FePt NPs. To investigate the composition distribution on the ferromagnetism of bigger FePt NPs, the as-synthesized 6 nm particles were annealed at 600°C for 1 h in vacuum in the experiments. The XRD pattern of the annealed sample was shown in Fig. 5a, the clear (110) peak as well as the shift of (111) peak from 40° to 41° indicate that ordered $L1_0$ structure is formed. Moreover, the narrow peaks in XRD spectrum suggest the growth of FePt particles during annealing. Figure 5b shows the hysteresis loop of the sample in Fig. 5a. The coercivity of the particles is 9.8 kOe at room temperature, which is close to the value reported by Chen [14]. Our results are consistent with Yu et al.'s study, suggesting that though inhomogeneous composition distribution exits in the isolated FePt NPs, its influence on the phase-transition of the particles can be mitigated by a "composition–compensation" process in thermal annealing. Namely, the Fe-rich nanoparticles could sinter with the Pt-rich particles nearby and thus give rise to the nearly equiatomic ratio of the FePt alloy nanocrystals. In the isolated FePt NP system, such "composition–compensation"

process could not happen and therefore the magnetic performance of the FePt NPs will be greatly affected by the composition distribution of the particles. These assumptions are supported by the relative low coercivitys for the annealed equiatomic FePt NPs with various separating matrix. For example, Caiulo et al. [19] employed a hydrothermal method to synthesize carbon encapsulated FePt nanoparticles which showed no severe coalescence by calcination at 900°C. However, the coercivity of the FePt nanoparticles is very definite. Held et al. [20] observed a dependence of coercivity on the thickness of the assembly layer in annealed FePt particle films. A low coercivity was observed for the monolayer particle films whereas the four-layer particle films showed higher coercivity with increased particle sintering. We recently fabricated isolated cubical FePt nanoparticle monolayers in the B_4C matrix, a coercivity of 2.2 kOe was obtained of the FePt nanoparticles in which a board composition distribution was found [21].

It should be noted that the formation mechanism of Fe_xPt_{1-x} depends on experimental parameters such as the choice of precursors for Fe and Pt, surfactants, solvents and flux time. Hence, the composition distribution of the FePt NPs is sensitive to the fabrication parameters. Recent literatures have shown that in the core–shell type FePt NPs, the inorganic shell could protect the inner FePt core from sintering during the annealing process and coercivity over 1T was obtained for the well-separated FePt NPs [22, 23]. These results suggest that the developed chemical synthesis allows precisely control over the composition variation as well as the uniformity of the FePt composited nanoparticles. In order to apply the FePt nanoparticles for various applications, especially for future ultrahigh-density data storage applications, direct access to the compositional distribution of the FePt NPs are also vital in future research.

Conclusions

In summary, we conducted a study on the composition distribution of FePt nanoparticles prepared by the oganometallic method, in which platinum acetylacetonate and Fe pentacarbonyl was used as precursors and oleyl amine and oleic acid as surfactants. We evidenced by STEM-EDX analysis that both the as-prepared 4.5 and 6.0 nm FePt nanoparticles have a wide compositional distribution, which is caused by the separation of nucleation and growth of particles in reaction. However, such wide composition distribution has limited influence on the ferromagnetism of sintering FePt nanoparticles through a "composition–compensation" process in thermal annealing.

Acknowledgments This work is supported in part by the National Nature Science Foundation of China under Grant No. 50801023 and 50801022, NSF, STD and ED of Hubei Province (No. 2007ABC005, No. 2009CDA035, No. 2008BAB010 and No. Z20091001).

References

1. S. Sun, C.B. Murray, D. Weller, L. Folks, A. Moser, Science **287**, 1989 (2000)
2. C.J. Xu, K.M. Xu, H.W. Gu, X.F. Zhong, Z.H. Guo, R.K. Zheng, X.X. Zhang, B. Xu, J. Am. Chem. Soc. **126**, 3392 (2004)
3. W. Chen, J. Kim, S.H. Sun, S.W. Chen, Langmuir **23**, 11303 (2007)
4. C. Wang, Y.L. Hou, J. Kim, S.H. Sun, Angew. Chem. Int. Ed. **46**, 6333 (2007)
5. H. Zeng, J. Li, Z.L. Wang, J.P. Liu, S.H. Sun, Nano. Lett. **4**, 187 (2004)
6. S. Qu, X.W. Zhang, Y. Gao, J.B. You, Y.M. Fan, Z.G. Yin, N.F. Chen, Nanotechnology **19**, 135704 (2008)
7. V. Nandwana, K.E. Elkins, N. Poudyal, G.S. Chaubey, K. Yano, J.P. Liu, J. Phys. Chem. C **111**, 4185 (2007)
8. S.S. Kang, G.X. Miao, S. Shi, Z. Jia, D.E. Nikles, J.W. Harrell, J. Am. Chem. Soc. **128**, 1042 (2006)
9. S. Yamamoto, Y. Morimoto, Y. Tamada, Y.K. Takahashi, K. Hono, T. Ono, M. Takano, Chem. Mater. **18**, 5385 (2006)
10. J.M. Qiu, J.P. Wang, Adv. Mater. **19**, 1703 (2007)
11. A.C.C. Yu, M. Mizuno, Y. Sasaki, H. Kondo, Appl. Phys. Lett. **85**, 6242 (2004)
12. H.G. Bagaria, D.T. Johnson, C. Sriastava, G.B. Thompson, M. Shamsuzzoha, D.E. Nikles, J. Appl. Phys. **101**, 104313 (2007)
13. C. Srivastava, J. Balasubramanian, C.H. Turner, J.M. Wiest, H.G. Bagaria, G.B. Thompson, J. Appl. Phys. **102**, 104310 (2007)
14. M. Chen, J. Kim, J.P. Liu, H.Y. Fan, S.H. Sun, J. Am. Chem. Soc. **128**, 7132 (2006)
15. J.Y. Dai, K. Li, P.F. Lee, X. Zhao, S. Redkar, Thin Solid Films **114**, 462 (2004)
16. S. Saita, S. Maenosono, Chem. Mater. **17**, 3705 (2005)
17. M. Delalande, P.R. Maroux, P. Reiss, Y. Samson, J. Mater. Chem. **17**, 1579 (2007)
18. B. Stahl, J. Ellrich, R. Theissmann, M. Ghafari, S. Bhattacharya, H. Hahn, N.S. Gajbhiye, D. Kramer, R.N. Viswanath, J. Weissmuller, H. Gleiter, Phys. Rev. B **67**, 14422 (2003)
19. N. Caiulo, C.H. Yu, K.M.K. Yu, C.C.H. Lo, W. Oduro, B. Thiebaut, P. Bishop, S.C. Tsang, Adv. Funct. Mater. **17**, 1392 (2007)
20. G.A. Held, H. Zeng, S.H. Sun, J. Appl. Phys. **95**, 1481 (2004)
21. H.B. Wang, M.J. Zhou, F.J. Yang, J. Wang, Y. Jiang, Y. Wang, H. Wang, Q. Li, Chem. Mater. **21**, 404 (2009)
22. J. Kim, C.B. Rong, J.P. Liu, S.H. Sun, Adv. Mater. **21**, 906 (2009)
23. Y. Tamada, S. Yamamoto, S. Nasu, T. Ono, Phys. Rev. B **78**, 214428 (2009)